EasyChair Preprint

№ 4839

Magnetic and Structural Characterizations of Pb and Sc Ions Doped MgO Nanoparticles by Modified Pechini Method

Israa A. Najem, Fadhil Abd Rasin and Shaker J. Edrees

December 29, 2020

Magnetic and Structural Characterizations of Pb and Sc Ions Doped MgO Nanoparticles by Modified Pechini Method

Israa A. Najem[1,4], Fadhil Abd Rasin[2] , Shaker J. Edrees[3]

[1] Technical Institution of Babylon, Al-Furat Al-Awsat Technical University, Iraq.
[4] Department of Materials Engineering, University of Technology, Baghdad, Iraq.
[2] Department of Materials Engineering, University of Technology, Baghdad, Iraq.
[3] Department of Ceramic & Building Materials Engineering, College of Materials Engineering, University of Babylon, Babylon, Iraq.

corresponding author's e-mail address: israadnan2000@gmail.com, inb.asr10@atu.edu.iq

Abstract. The Room Temperature Ferromagnetic (RTFM) were discussed in the present paper of the undoped and the doped samples with different content of Pb^{2+} ions and Sc^{+3} ions. The modified pechini method was used to prepare the pure and the doped samples ($Mg_{0.097}Pb_{(0.03-y)}Sc_yO$)-NPs, where ($0.01 \leq y \leq 0.03$). The structural, morphological, chemical composition and magnetic properties of the samples were characterized by X-Ray Diffraction (XRD), Field Emission Scanning Electron Microscopy (FE-SEM), Energy Dispersive Spectroscopy (EDS) and Vibrating Sample Magnetometer (VSM) respectively. The XRD patterns showed that the synthesized materials have a single set of peaks, which corresponding the cubic phase of MgO-NPs. The lattice parameter, the interplanner spacing and the crystallite size were varied according to different dopant concentration of Sc^{+3} ions and Pb^{2+} ions in the MgO-NPs host lattice for doped samples. Furthermore, the intensity was reduced. The morphology of pure and doped samples showed small spherical nanoparticles with particle size (22.87-19.725nm) by employing the FE-SEM. The purity of all the samples was confirmed by using EDS spectroscopy. Magnetic measurements by (VSM) revealed that all the samples offer room temperature ferromagnetism (RTFM). The saturation magnetism of (Ms) was found to be varied as a function of doping concentration, which may be attributed to local magnetization supported by F-center mechanism. The maximum (Ms) was found for the $Mg_{0.97}Sc_{0.03}O$ sample. The obtained results suggest that both Pb^{2+} ions and Sc^{+3} ions doping and oxygen vacancies play an remarkable role in the development of room temperature ferromagnetism, which may be convenient for spintronic application.

Keywords: doping, MgO-NPs , PbO, ScO, Pechini, RTFM, VSM.

1. Introduction

The study of nanoparticles show novel properties, which are dissimilarity from those of bulk materials, the unique properties and the efficient performance of nano materials are determined by their surface structure, size and particle interaction [1][2]. Nano materials have a considerable prominent surface area to volume proportion than their traditional structures, which can be prompted more noteworthy effect their quality and synthetic reactivity [3]. The role play by particle size is similar, in some cases, to the particle chemical composition, by adding another parameter for designing and controlling their behaviour [1]. The promise of nanocrystals as a technological material for applications including magnetic [4], bio[5], and fuel cells [6] may ultimately be based on tailoring their behaviour by adding impurities through doping.

Therefore, it is a motivating from a technological point of view to dope oxide semiconductors with various ions besides rare earth ions to view the possibility of the existence of optical and magnetic properties [7], which is an important tool for the modification [8]. Dopants in nanocrystals lead to phenomena not existent

in the bulk because their electronic states are bounded to a small volume [9]. However, the dopant impurities is tuned the properties of metal oxide nanoparticles such as MgO.[10][11][12], which can be altered the properties, as in demand for their industrial applications as optical and magnetic sensor, switching device and as diluted magnetic semiconductor [10][13], by modification the energy gap [14][15], the magnetic properties [16][17], the antibacterial effect [18], the optical [19][16], the conduction [20] and the Photoluminescence [21].

Ferromagnetism is induced by lattice defects or nonmagnetic impurities have attracted considerable interests in the area of spintronics [22], which is a field of science and technology that contributions novel electronic devices [23]. Such as (spin-LEDs) spin light-emitting diodes, (spin-FETs) spin field effect transistors and spin qubits for quantum computers [24].

This magnetization called "d^0 ferromagnetism" is a modern class of magnetism, in which the ferromagnetism contain no magnetic elements together with partially filled d or f shells [23][25]. These observations can be established in rocksalt structure (HfO, MgO, CaO and Al_2O_3) which do not include ions with partially filled d or f bands [26].

MgO is one of the most attractive model materials for inspect "d^0 ferromagnetism", which can produce a spin-polarized p band due to its wide band gap [23]; however, the MgO-NPs is confirmed the RTFM while the bulk MgO is nonmagnetic [27][28].

Many experimental and theoretical record on observations of the origin of RTFM in MgO-NPs [29][30], such magnetization is not demanded on the existence of free carriers for the observed magnetic fingerprints in MgO-NPs [26], but it strongly indicating that RTFM property is intrinsic in nature and strongly correlates to the defects and oxygen vacancies due to rare earth and transition metal cations doping. Doping with transition ions that have partly filled d states (Mn, Cu, V, Cr, Fe, Co, Ti, Ni, and Sc) and rare earth elements that have partly filled f states (Er, Gd, Eu). This transition ions have been utilized as magnetic atoms in diluted magnetic semiconductor DMS [31]. The partly filled d states or f states include unpaired electrons, in terms of their spin, which are responsible for them to display magnetic behaviour [22].

So the source of magnetism is correlating with the presence of a little concentration of intrinsic point impurities isolated cation vacancies driving to the forming of high-spin defect sites [32]. There are no valence d electrons in rocksalt structure. Hence the valence band is controlled by O-2p orbitals. [23][32][33].

Several preparation routes used to prepare pure and doped MgO-NPs, such as combustion [34], aerogel route [35], hard templating path way [36], microwave sol-gel method [37], Liquid-Phase Method [38], Co-precipitation [39], green synthesis [40], sol-gel method [18], Modification of Pechini sol–gel process [41], spinning disk reactor [42].

Among the overall number of chemical synthesis methods obtainable for preparation of pure\doped MgO-NPs, Pechini method was favourite one due to it's important in the synthesis of magnetic materials, high temperature superconductors, ceramics and catalysts [43]. The preference of this method include good stoichiometric control, good homogeneity and good control of particle morphology [44].

The main objective of this work is to detect the effect of different content of Pb^{2+} ions and Sc^{3+} ions that incorporated into the crystal structure of MgO-NPs, where all the samples were prepared by modified Pechini method. In order to obtain a better understanding of current work, the XRD, FE-SEM coupled with EDX and VSM tests were investigated to go after changes that take place in the structure with the variation fraction of doping.

2. Experimental Method

2.1. Chemical Used

Magnesium nitrate hexahydrate ($Mg(NO_3)_2 \cdot 6H_2O$) [BDH Chemicals Ltd, England, > 99% purity], lead nitrate ($Pb(NO_3)_2$) [Chemicals PVT, India, > 99% purity], $Sc(NO_3)_3$ [Ganzhou Wanfeng Advanced Materials Technology Co., Chaina, Ltd., > 99% purity], citric acid ($C_6H_8O_7.H_2O$) [CDH, India, >99%], Ethelyen Glygol, EG, ($CH_2(OH).CH_2OH$) [Chemicals PVT. LTD, India, > 99% purity] and distilled water

were involved to prepare ($Mg_{0.097}Pb_{(0.03-y)}Sc_yO$)-NPs samples, where ($0.01 \leq y \leq 0.03$). using modified pechini method. All raw chemical materials were used without any further purifications.

2.2. Samples Preparation

2.2.1. Synthesis of MgO-NPs Nanoparticles. The procedure of the synthesis MgO-NPs involved the preparation of a stable aqueous solution of the metal salt starting with magnesium nitrite solution and the tricarboxylic acid as citric acid solution were dissolved separately in an adequate amount of the deionized water (100 ml) for each of them, in a molar ratio of 1:1, stirred for 1 hour under constant stirring (FALC instrument-F91). Then citric acid was added into a magnesium nitrite solution to chelate Mg^{2+} ions in the solution, however the resulting solution was kept at 90°C for three hours under constant stirring. EG was added with fixed mass ratio, CA/EG, 2:3. The colour of the final mixed solutions was gradually changed into yellowish, as a result of water evaporation. Finally formation a very viscous gel with brown colour. The dehydrated gel was calcinated at a moderate temperature 420°C for 2 hours with 3°C/min as a heating rate using a furnace device (PIF 160/15- Made in Turkey) to form a loose powder.

The procedure of synthesis ($Mg_{0.097}Pb_{(0.03-y)}Sc_yO$)-NPs doped samples, where ($0.01 \leq y \leq 0.03$), was involved the preparation of an extra stable aqueous solution of lead nitrite and scandium nitrite, which were dissolved separately in an adequate amount of the deionized water under constant stir for 1 hour. The citric acid was added into a mixed solutions of the magnesium nitrite, lead nitrite and scandium nitrite to chelate Mg^{2+}, $Pb^{2+}$and Sc^{+3} in the solution. Continuous the same procedure steps of preparation MgO-NPs sample to obtain ($Mg_{0.097}Pb_{(0.03-y)}Sc_yO$)-NPs powder samples.

3. Characterization Techniques

All the seven samples of undoped and doped ($Mg_{0.097}Pb_{(0.03-y)}Sc_yO$)-NPs samples, where ($0.01 \leq y \leq 0.03$),. were analysed by powder XRD, FE-SEM coupled with EDS analysis and VSM. Powder X-Ray Diffraction (XRD) patterns were gained using Shimadzu-6000 diffractometer with Cu-Kα radiation (λ=1.5406Å). The surface morphology of nanoparticles samples were investigated using a field emission scanning electron microscope(FESEM) (TESCAN MIRA3 FEG-SEM) operating at 30kV coupled with an energy-dispersive spectroscopy (EDS) instrument for elemental analysis. The magnetic measurements were achieved using a vibrating sample magnetometer (VSM) type cryogenic device at room temperature.

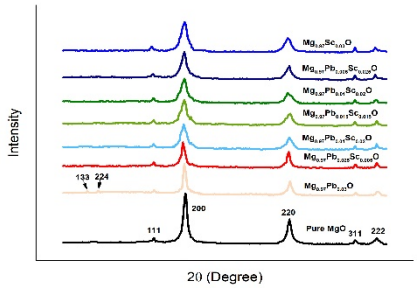

Figure 1. XRD analysis for ($Mg_{0.097}Pb_{(0.03-y)}Sc_yO$)-NPs samples calcined at 420°C for 2 hours.

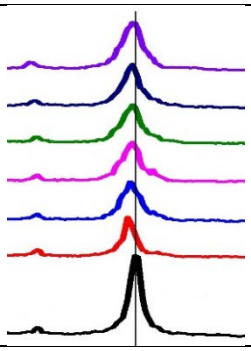

Figure 2. XRD shifting for pure and doped ($Mg_{0.097}Pb_{(0.03-y)}Sc_yO$)-NPs samples.

4. Result and Discussion

4.1. Structural Analysis X-ray diffraction (XRD)

A powerful non-destructive technique was used to characterize crystalline materials. XRD technique can provide an information on phases, structures, preferred crystal orientations and other structural parameters, such as crystallinity, width, average grain size and the intensity of the diffraction peaks which depend on lattice strain. The powder, of as prepared ($Mg_{0.097}Pb_{(0.03-y)}Sc_yO$)-NPs samples by modified pechini method calcianed at 420°C for 2 hours, was investigated by employing XRD technique.

Figure (1). reveals that the reflections resultant of the ($Mg_{0.097}Pb_{(0.03-y)}Sc_yO$)-NPs samples are indexed well to the cubic phase of MgO, having space group Fm3m (#225). The five major diffraction peaks confirm the existence of pure MgO-NPs, which can be seen at the position 36.6325, 42.6868, 61.9761, 74.3027, 78.2192, conformable to the lattice planes (111), (200), (220), (311) and (222). All the ($Mg_{0.097}Pb_{0.03-y}Sc_yO$)-NPs samples were matched with [ICSD PDF code 01-075-0447]. This results are in line with earlier reports[16][18].

For pure structure of MgO-NPs, the strongest diffraction peak (200) is positioned at 42.6868, while the position of doped samples with different content of Pb^{2+} ions and with Sc^{+3} ions are observed shifting to a lower 2θ peaks positions as cleared from the figure (2). This slightly shifted peak position towards less 2θ values can be ascribed due to the ionic radius difference between Pb^{2+} (1.19 Å) ions, Sc^{+3} (0.745 Å) and Mg^{2+} (0.72 Å) ions.

The figure.(2) shows the shifting of the pure and doped samples. The samples that doped with high fraction of Pb^{+2} ions are shifting more than the samples that doped with high fraction of Sc^{+3}ions.

The shifting in the diffraction peak positions establishes substitution effects and denotes a structural change due to the lattice distortion caused by the dopant ions [45].

The incorporation of different content of Pb^{2+} ions and Sc^{3+} ions into the crystal structure of MgO-NPs can be caused changes in the interplaner d-spacing. This can be related to the doped samples as cleared in table (1), such dopants can be caused strain in the lattice of compounds [13][18].

An introduction of the dopants with different ionic radius in the host lattice atoms cause lattice contraction or expansion. One observes from figure (2) that the diffraction peaks shift lightly in the position indicating a light change in the lattice parameter. This variation in the lattice constant is proportional to the ionic radius difference between the dopants and substituted host lattice and to the concentration of the dopants [46]. It is cleared from the table (1), that the lattice parameter is increased at first and then decreased. The lattice parameter for pure MgO-NPs is (4.22832Å), while it is larger in values for the doped samples. Such behaviour can be attributed to the ionic radius difference between the dopants and the MgO host lattice.

It is also evident from Figure 2 that the intensity of the strongest diffraction peak (2θ=42.643468) along (200) plane decreased and the full width at half maximum (FWHM) increased when different content of Pb^{2+} ions and Sc^{+3}ions were doped [47]. This indicating that the undoped sample had a better phase purity and crystallinity and Pb^{2+} ions and Sc^{+3}ions were successfully replaced Mg^{2+} ions in the MgO-NPs host lattice due to the change in the scattering centers of the the doped samples [48]. The intensity of the XRD peaks can be affected by the composition including occupancy of atomic sites, the scattering ability of constituent atoms, and fractional coordinates [18][49][50].

In order to determine the average crystallite size (D). the Scherrer's formula was used to evaluate the the average crystallite size of pure and doped MgO-NPs samples along (220) and (200) planes [51].

$$D = \frac{K\lambda}{\beta cos\theta} \dots\dots\dots\dots (1) \qquad (1)$$

where (D) is the crystallite size, (λ) the X-ray wavelength of the copper anode (1.5406Å), k the shape factor (k = 0.9), (β) the full width at half maximum (FWHM) of the diffraction peaks, and (θ) the Bragg diffraction angle[52].

The crystallite size is varied according to doping different content of Pb^{2+} ions Sc^{+3}ions as cleared from table (1).The smallest value in the crystallite size has been recorded for the ($Mg_{0.97}Sc_{0.03}O$) sample that have the maximum fraction of Sc^{+3} ions and it is free from Pb^{2+} ions. This can be related to the decrease in the grain growth after doping with trivalent rare-earth ions ,Sc, which can be acted as a grain growth inhibitors [53].
The XRD peak broadening in the doped samples emphasizes the decrease in the crystallite sizes of the doped samples [48][53].

TABLE 1. Structural parameters of pure and doped MgO-NPs calcined at 420 °C.

	Crystallite Size nm	**Lattice Parameter**	**d**
MgO	5.693325	4.22832	2.11949
$Mg_{0.97}Pb_{0.025}Sc_{0.005}O$	6.89561	4.23996	2.12397
$Mg_{0.97}Pb_{0.02}Sc_{0.01}O$	5.44299	4.23965	2.12345
$Mg_{0.97}Pb_{0.015}Sc_{0.015}O$	5.33956	4.23921	2.12337
$Mg_{0.97}Pb_{0.01}Sc_{0.02}O$	5.113225	4.23766	2.12334
$Mg_{0.97}Pb_{0.005}Sc_{0.025}O$	5.030591	4.23696	2.12323
$Mg_{0.97}Sc_{0.03}O$	4.792012	4.22859	2.12109

4.2 Morphology Analysis
The Field Emission Scanning Electron Microscope (FE-SEM) technique was employed to explore the size and the distribution of all the samples. The images in the figure (3,4,5,6,7,8,9-a) display the morphology of the synthesized ($Mg_{0.097}Pb_{(0.03-y)}Sc_yO$)-NPs samples by using the modified pechini method. The images display agglomeration of the spherical nanoparticles, which occurs due to high surface energy of the nanoparticles. The capability to produce agglomeration is very strong, which is increased the collision frequency between particles, that lead to a higher degree of the agglomeration. Chemical bonds may form between the particle surfaces as van der Waals forces, which are always present. Additionally, the magnetic dipole forces can be potentially participated to the internal particle forces[54][55].
The average grain size for all the seven samples under investigation is in the range (22.87-19.725nm) as clear from the statically histogram in the figure (3,4,5,6,7,8,9-b). The grain size start to decreases with the increase the fraction of doping Sc^{+3} ions and with the decrease or absence of doping Pb^{2+} ions., which is in a good convention with the crystallite size determined from the XRD and statically histogram.

4.3 Energy-dispersive X-ray Spectroscopy EDS
The Energy Dispersion Spectroscopy (EDS) analysis was utilized to confirm the composition of the prepared nanocrystals samples , which is usually coupled with the FE-SEM instrument. The EDS is a very useful technique for qualitative and quantitative analysis of relative concentration of the element [56]. The EDS spectroscopy, which was used to detach the pure and the doped MgO-NPs with different content of Pb^{2+} ions and Sc^{3+} ions that synthesis by modifying pechini method. as shown in the figure (3,4,5,6,7,8,9-c). The EDS spectrum for the pure MgO-NPs sample just confirm the presence of the Magnesium (Mg) and Oxygen (O) as the only elements, that demonstrate the high purity of the nano powder. The a partially higher oxygen atomic ratio as compared to that of magnesium is possibly because of moisture absorption from the environment [57].
The EDS analysis of the doped ($Mg_{0.097}Pb_{(0.03-y)}Sc_yO$)-NPs samples in the figure (3,4,5,6,7,8,9-c) confirm the presence of the Mg, Pb, Sc and O as the only elementary components with the absence of any extra element.

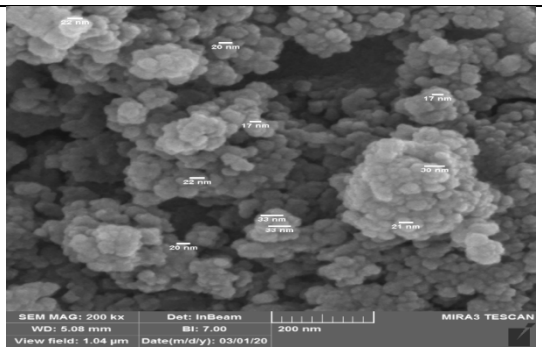

a.

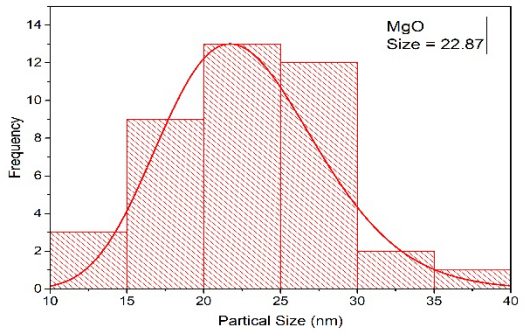

b.

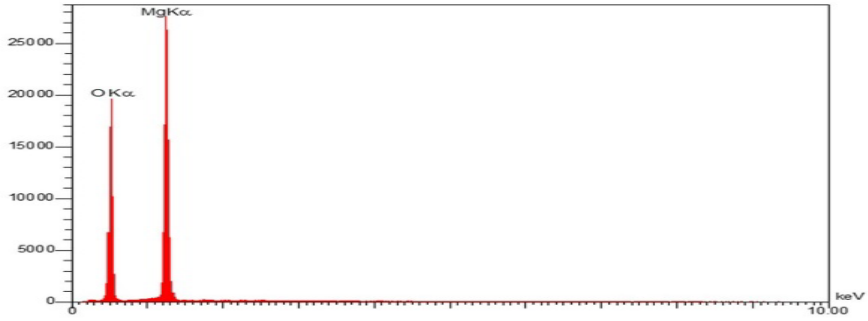

c.

Figure 3. MgO-NPs sample a. FE-SEM sample, b. Histogram and c. EDS.

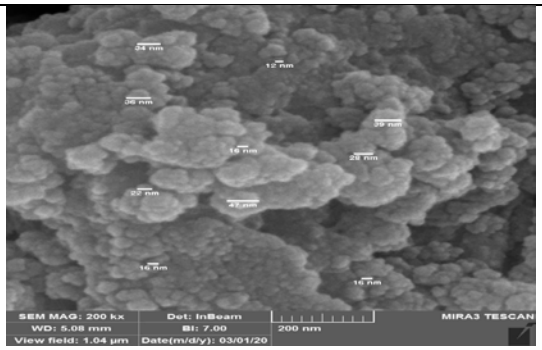

a.

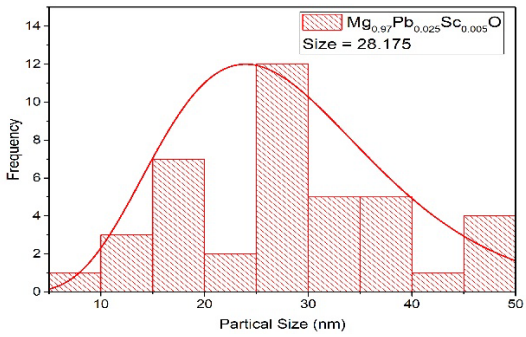

b.

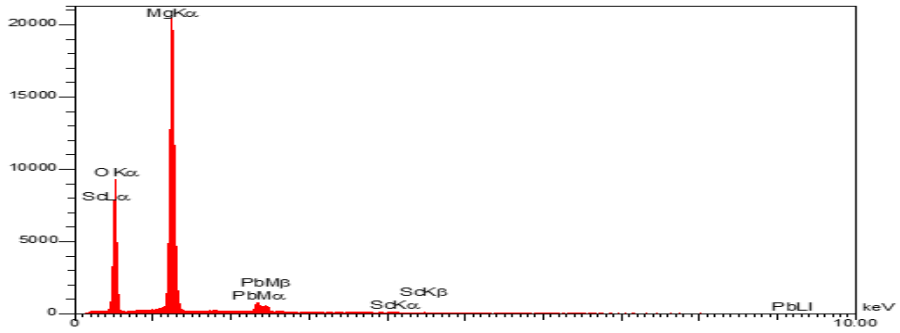

c.

Figure 4. ($Mg_{0.097}Pb_{0.025}Sc_{0.005}O$)-NPs samples a. FE-SEM sample, b. Histogram and c. EDS.

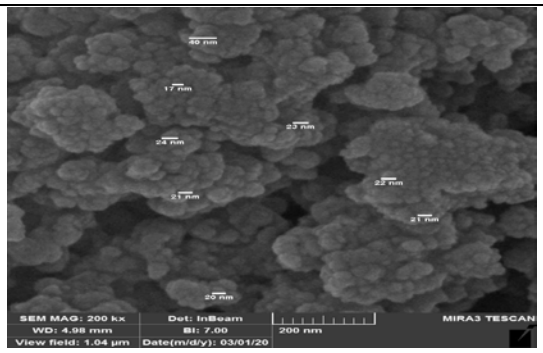

a.

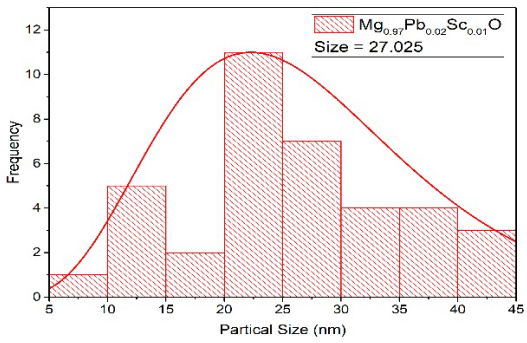

b.

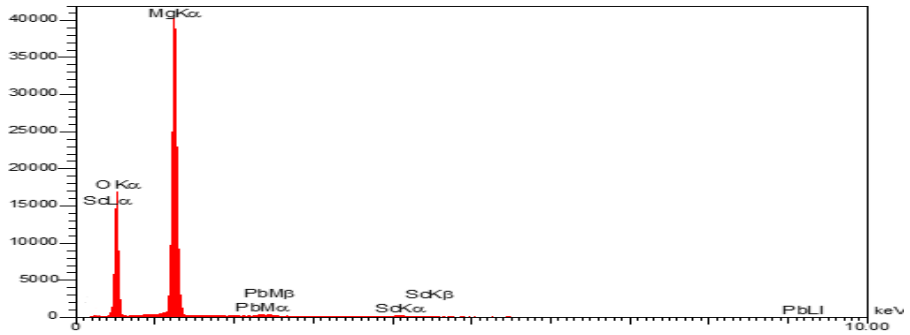

c.

Figure 5. ($Mg_{0.097}Pb_{0.02}Sc_{0.01}O$)-NPs samples a. FE-SEM sample, b. Histogram and c. EDS.

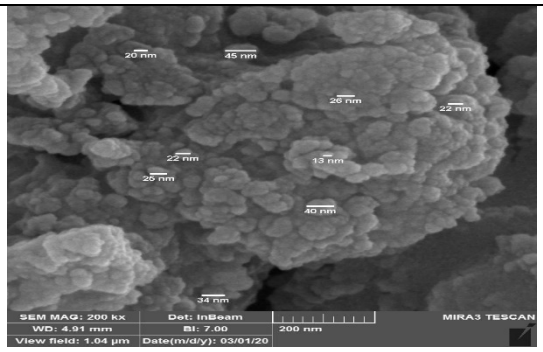

a.

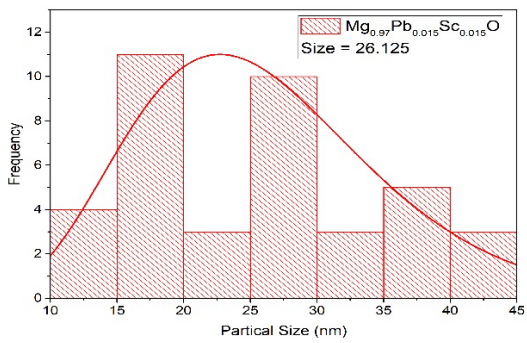

b.

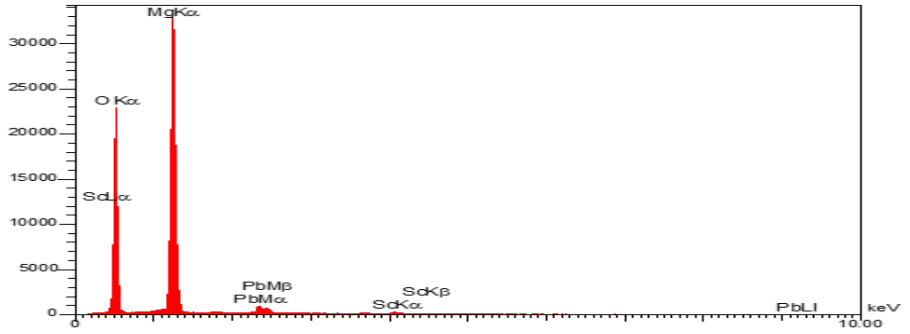

c.

Figure 6. MgO-1.5% ($Mg_{0.097}Pb_{0.015}Sc_{0.015}O$)-NPs samples a. FE-SEM sample, b. Histogram and c. EDS.

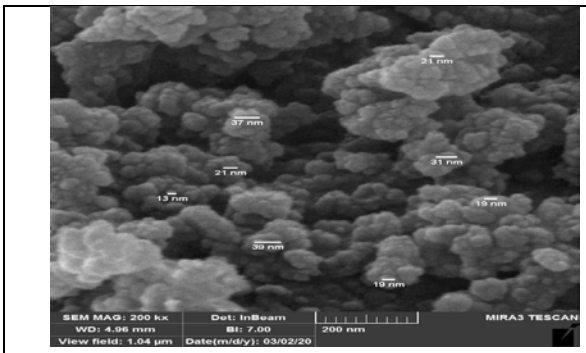

a.

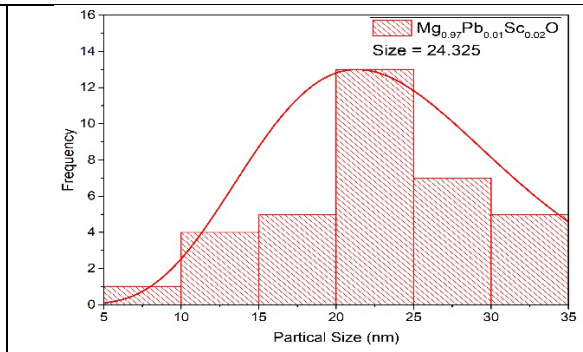

b.

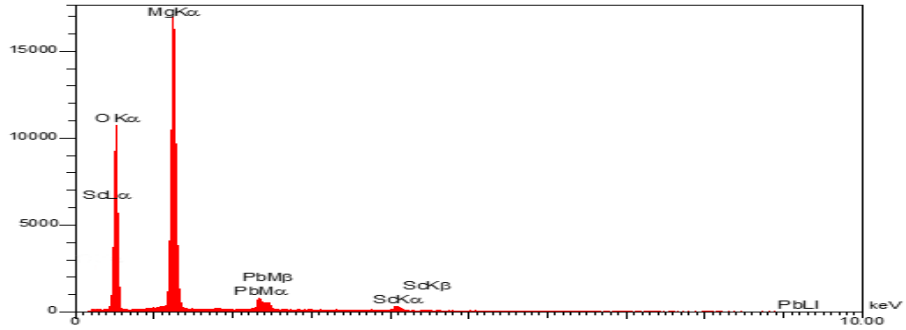

c.

Figure 7. MgO-2% ($Mg_{0.097}Pb_{0.01}Sc_{0.02}O$)-NPs samples a. FE-SEM sample, b. Histogram and c. EDS.

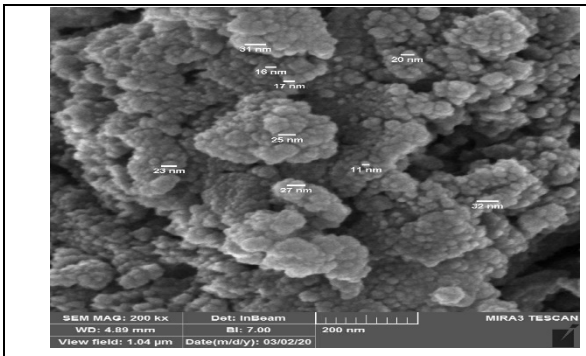

a.

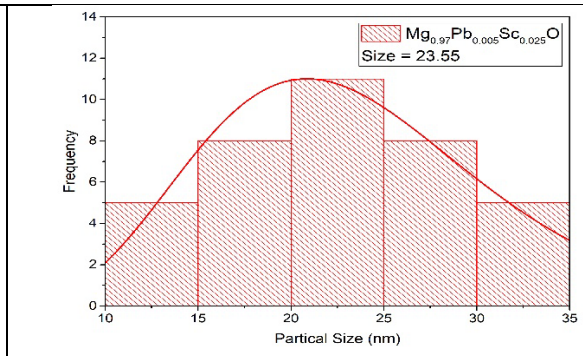

b.

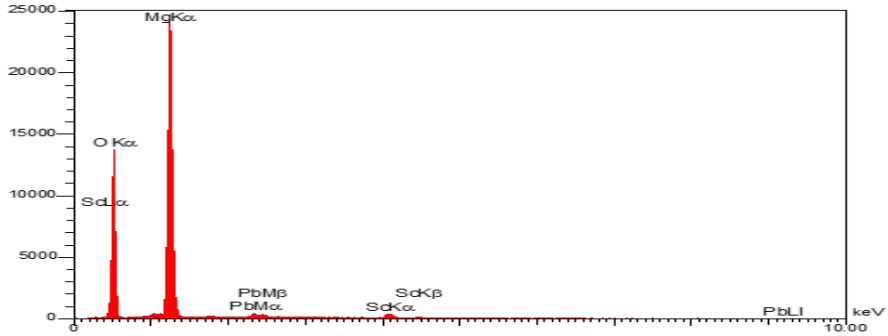

c.

Figure 8. MgO-2.5% ($Mg_{0.097}Pb_{0.005}Sc_{0.025}O$)-NPs samples a. FE-SEM sample, b. Histogram and c. EDS.

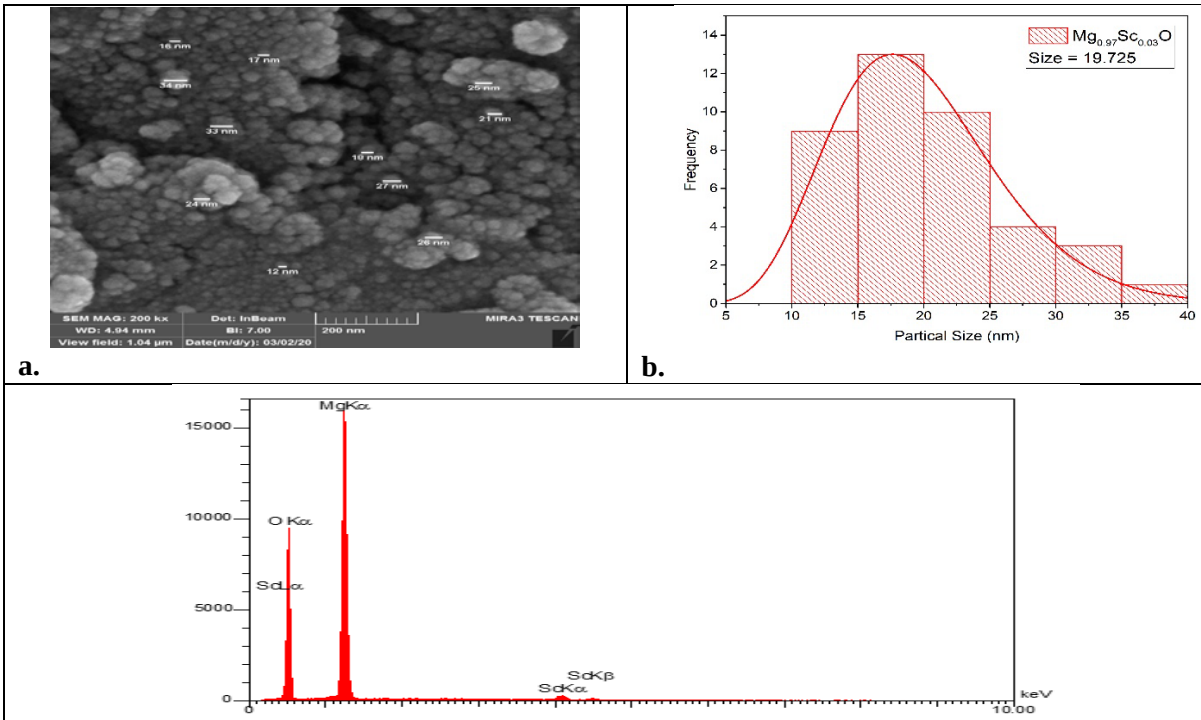

Figure 9. MgO-3% ($Mg_{0.097}Sc_{0.03}O$)-NPs samples a. FE-SEM sample, b. Histogram and c. EDS.

4.4 VSM Magnetization

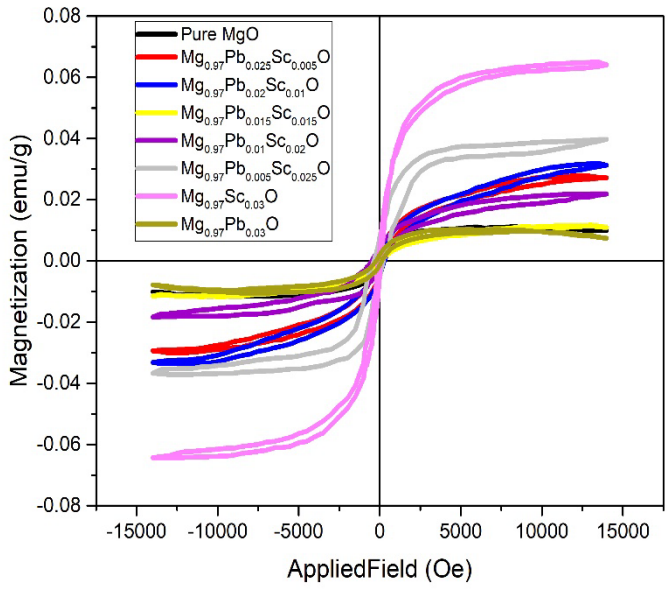

Figure 10. VSM for undoped and doped ($Mg_{0.097}Pb_{(0.03-y)}Sc_yO$)-NPs samples.

The magnetization behaviour curves in figure (10) for prepared nanocrystallites ($Mg_{0.097}Pb_{(0.03-y)}Sc_yO$) samples by modified pechini method were performed to study the effects of the Pb^{+2} ions and the Sc^{+3} ions substitution on inducing magnetism in MgO-NPs host lattice. The undoped and doped samples calcined at 420°C for 2 hours were investigated by vibrating samples magnetometer (VSM). The VSM shows the hysteresis loops for the seven samples that have been investigated at room temperature and motivated by the defects. The Room Temperature Ferromagntism RTFM can be observed in MgO-NPs with a particle size of (10–50 nm) [58], which was confirmed by a crystallite size and a particle size from XRD analysis and the statically histogram of FE-SEM respectively.

The origin of ferromagnetism in MgO is assumed to be resulting from the oxygen vacancies at the surface of the nanoparticles [59]. The magnetic order in the lattice of the pure and the doped MgO-NPs samples can be achieved by providing a certain density of vacancies, which can consider the necessary condition for ferromagnetism. Such vacancies or other defects in the lattice were achieved nearly localized magnetic moments [60]. This vacancies were usually labeled as F and V centers, which corresponding to the missing oxygen atom or Mg atom respectively, in the host lattice of MgO-NPs [61].

The reason behind the encouraging magnetic moment was spin polarization of 2p electrons of O atoms that is close to the negative charge VMg [27][32]. However, The cations were enclosed by an octahedron of anions with filled valence p bands and the bonding anion p orbitals with lobes point to the cation site would be the generality energetically favoured attraction orbitals to provide the vacancies. So that the vacancies were necessary to charge recompense by a cation vacancy at the center of such an octahedron [28][62].

From the figure (10) all the seven samples of undoped and doped MgO-NPs exhibit RTFM hysteresis loop. The observed ferromagnetism in Pb^{+2} and Sc^{+3} doped MgO can be explained by using the F-centre exchange coupling (FCE), in which both the doped ions (Pb^{+2} and Sc^{+3}) and the oxygen vacancy are involved. According to the FCE mechanism, oxygen vacancy and the ion are two requisite requirements, which results the FM ordering [59].

The undoped MgO-NPs as well as in other undoped oxide semiconductors, can be resulted from the interchange interactions between electron spin moment of Mg^{+2} ions and the V_O at the particle surface, where Vo represent oxygen vacancies [63].

The variation in the magnetization for doped samples can understand according to the FCE mechanism, in which the electron can be trapped in oxygen vacancy to form F-centre. The oxygen vacancy constitutes two groups with two Pb^{2+} ions (Pb^{2+}-Vo-Pb^{2+}) and with two Sc^{3+} ions (Sc^{3+}-Vo-Sc^{3+}), An electron trapped in oxygen vacancy take an orbital, that overlaps the shell of neighboring Sc^{3+} ions. According to the principle of Hund's rule and Pauli principle, the trapped electrons spin should have a parallel direction to two neighboring, thus the ferromagnetic ordering can be achieved [64]. Moreover, the doping of divalent and trivalent ions may lead more oxygen vacancy in doped MgO in order to maintain the charge neutrality. So that the ions that enter substitutionally in place of Mg^{+2} in the lattice produce an oxygen vacancies. These oxygen vacancies are accountable for the FM behaviour in these samples[64].

It is observed from figure (10) that the saturation magnetization initially increase for the samples ($Mg_{0.97}Pb_{0.025}Sc_{0.005}O$) and ($Mg_{0.97}Pb_{0.02}Sc_{0.01}O$) with the increasing of Sc^{+3} ions and decrease of Pb^{+2} ions concentration in the MgO host lattice as compared with the undoped MgO-NPs sample. Due to a small separation between Pb^{+2} and Sc^{+3} ions which results increase of local magnetization with the Pb^{+2} and Sc^{+3} groups, which are mediated by FCE interactions [63], and then start to decrease for the samples ($Mg_{0.97}Pb_{0.015}Sc_{0.015}O$) and ($Mg_{0.97}Pb_{0.01}Sc_{0.02}O$), suggesting that further increase in the Sc^{+3} ions and decrease in the Pb^{+2} ions may results super-exchange interactions between Pb^{+2} and Sc^{+3} ions mediated by oxygen ions. This super-exchange interaction results the antiferromagnetic ordering, which minimize the FM ordering in the Pb^{+2} and Sc^{+3} doped MgO host lattice [63].

Then the (Ms) begin to increase again for the samples ($Mg_{0.97}Pb_{0.005}Sc_{0.025}O$) and ($Mg_{0.97}Sc_{0.03}O$) and the maximum (Ms) appears for the ($Mg_{0.97}Sc_{0.03}O$) sample, that is free from pb^{+2} ions. This long-range ferromagnetic ordering can be motivated via a number of causes, such as increased F centers, dangling bonds, ion vacancies, intercrystalline grains, unpaired electrons are establish in crystallites, or at the surface/interfaces [65].

5. Conclusion

The undoped and doped samples have been successfully synthesized via modified Pechini method with different content of Pb^{+2} ions and Sc^{+3} ions.

the undoped and the doped ($Mg_{0.097}Pb_{(0.03-y)}Sc_yO$)-NPs samples ($0.01 \leq y \leq 0.03$) were calcinated 420°C for 2 hours with 3°C /min as a heating rate.

Single cubic phase with space group Fm3m (#225) has been confirmed for undoped and doped samples by employing the resultant powder to XRD instrument. As a result of varying the fraction of doping, the strongest diffraction peak (200) has been shifted towards lower 2θ values and the interplaner d-spacing, lattice parameter, crystallinity have been changed according to dopants concenteration. Furthermore, the intensity has been reduced. This can be attributed to the ionic radius difference between Pb^{2+}(1.19 Å), Sc^{+3} (0.745 Å) and Mg^{2+} (0.72 Å) ions.

The morphology of the surface for the pure and the doped nanoparticles samples has been display spherical nanoparticles shape. The average grain size (22.87-29.05nm) has been varied according to the content of the dopants concentration as was confirmed by statically histogram and crystallinity from XRD.

The EDS has been confirmed the presence of Mg, Pb, Sc and O as the only elementary components.

The hysteries loop revaled that all the samples exhibited RTFM ordering. The observed FM is well explained due to involve both oxygen vacancy and Pb^{2+} ions and transition Sc^{+3} ions by using the F-centre exchange coupling mechanism (FCE).The pure MgO-NPs assure the formation of RTFM. The maximum (Ms) appears for the ($Mg_{0.97}Sc_{0.03}O$) sample that is free from pb ions. This improves some guide for codoping Pb^{+2} ions and transition Sc^{+3} ions in MgO to distinguish FM in this system. With the ability to create Pb^{+2} ions and transition Sc^{+3} ions doped MgO with a better magnetization at room temperature, it is a promising material for employ in possible spintronic devices.

6. References

[1] Wang ZL. Characterization of nanophase materials. vol. 18. 2001. https://doi.org/10.1002/1521-4117(200110)18:3<142::AID-PPSC142>3.0.CO;2-N.

[2] Greim (Chairman) H. Constitution and Procedures of the Commission for the Investigation of Health Hazards of Chemical Compounds in the Work Area. 2004. https://doi.org/10.1002/3527600418.make016.pub2.

[3] Iqbal T, Tufail S, Ghazal S. Synthesis of Silver, Chromium, Manganese, Tin and Iron Nano Particles by Different Techniques. Int J Nanosci Nanotechnol 2017;13:19–52.

[4] Shabatina TI, Vernaya OI, Shabatin VP, Melnikov MY. Magnetic Nanoparticles for Biomedical Purposes: Modern Trends and Prospects. Magnetochemistry 2020;6:30. https://doi.org/10.3390/magnetochemistry6030030.

[5] Thomas S, Harshita BSP, Mishra P, Talegaonkar S. Ceramic Nanoparticles: Fabrication Methods and Applications in Drug Delivery. Curr Pharm Des 2015;21:6165–88. https://doi.org/10.2174/1381612821666151027153246.

[6] Tarutin A, Danilov N, Lyagaeva J, Medvedev D. One-step fabrication of protonic ceramic fuel cells using a convenient tape calendering method. Appl Sci 2020;10. https://doi.org/10.3390/app10072481.

[7] Thangeeswari T, Priya M, Velmurugan J. Enhancement in the optical and magnetic properties of ZnO:Co implanted by Gd3+ nanoparticles. J Mater Sci Mater Electron 2015;26:2436–44. https://doi.org/10.1007/s10854-015-2703-2.

[8] Elimelech O, Liu J, Plonka AM, Frenkel AI, Banin U. Size Dependence of Doping by a Vacancy Formation Reaction in Copper Sulfide Nanocrystals. Angew Chemie 2017;129:10471–6. https://doi.org/10.1002/ange.201702673.

[9] John R, Rajakumari R. Synthesis and Characterization of Rare Earth Ion Doped Nano ZnO. Nano-Micro Lett 2012;4:65–72. https://doi.org/10.1007/bf03353694.

[10] Misra D, Yadav SK. Prediction of Site Preference of Implanted Transition Metal Dopants in Rock-salt Oxides. Sci Rep 2019;9. https://doi.org/10.1038/s41598-019-49011-5.

[11] Erwin SC, Zu L, Haftel MI, Efros AL, Kennedy TA, Norris DJ. Doping semiconductor nanocrystals. Nature 2005;436:91–4. https://doi.org/10.1038/nature03832.

[12] Sharma U, Jeevanandam P. Synthesis of Zn2+-doped MgO nanoparticles using substituted brucite precursors and studies on their optical properties. J Sol-Gel Sci Technol 2015;75:635–48. https://doi.org/10.1007/s10971-015-3734-0.
[13] Vasanthi V, Kottaisamy M, Anitha K, Ramakrishnan V. Near UV excitable yellow light emitting Zn doped MgO for WLED application. Superlattices Microstruct 2017;106:174–83. https://doi.org/10.1016/j.spmi.2017.03.050.
[14] Sharma U, Jeevanandam P. Layered double hydroxides as precursors to Ti4+ doped MgO nanoparticles with tunable band gap. J Nanosci Nanotechnol 2018;18:264–78. https://doi.org/10.1166/jnn.2018.14557.
[15] Lee JW, Ko JH. Defect states of transition metal-doped MgO for secondary electron emission of plasma display panel. J Inf Disp 2014;15:157–61. https://doi.org/10.1080/15980316.2014.955140.
[16] Azzaza S, El-Hilo M, Narayanan S, Judith Vijaya J, Mamouni N, Benyoussef A, et al. Structural, optical and magnetic characterizations of Mn-doped MgO nanoparticles. Mater Chem Phys 2014;143:1500–7. https://doi.org/10.1016/j.matchemphys.2013.12.006.
[17] Fox GT, Wolfmeyer MW, Dillinger JR, Huber DL. Magnetic field dependence of the thermal conductivity of doped MgO. Phys Rev 1968;165:898–901. https://doi.org/10.1103/PhysRev.165.898.
[18] Cai Y, Wu D, Zhu X, Wang W, Tan F, Chen J, et al. Sol-gel preparation of Ag-doped MgO nanoparticles with high efficiency for bacterial inactivation. Ceram Int 2017;43:1066–72. https://doi.org/10.1016/j.ceramint.2016.10.041.
[19] Sharma U, Jeevanandam P. Synthesis of Zn2+-doped MgO nanoparticles using substituted brucite precursors and studies on their optical properties. J Sol-Gel Sci Technol 2015;75:635–48. https://doi.org/10.1007/s10971-015-3734-0.
[20] Kim B, Lee H. Valence state and ionic conduction in Mn-doped MgO partially stabilized zirconia. J Am Ceram Soc 2018;101:1790–5. https://doi.org/10.1111/jace.15333.
[21] Peng L, Wang Y, Wang Z, Dong Q. Multiplesite structure and photoluminescence properties of Eu3+ doped MgO nanocrystals. Appl Phys A Mater Sci Process 2011;102:387–92. https://doi.org/10.1007/s00339-010-6027-z.
[22] Kuang FG, Kang SY, Kuang XY, Chen QF. An ab initio study on the electronic and magnetic properties of MgO with intrinsic defects. RSC Adv 2014;4:51366–73. https://doi.org/10.1039/c4ra06340f.
[23] Hu J, Zhang Z, Zhao M, Qin H, Jiang M. Room-temperature ferromagnetism in MgO nanocrystalline powders. Appl Phys Lett 2008;93:1–4. https://doi.org/10.1063/1.3021085.
[24] Ahmed SA. Room-temperature ferromagnetism in pure and Mn doped SnO2 powders. Solid State Commun 2010;150:2190–3. https://doi.org/10.1016/j.ssc.2010.08.029.
[25] Xue D, Chai G, Li X, Fan X. Effects of grain size distribution on coercivity and permeability of ferromagnets. J Magn Magn Mater 2008;320:1541–3. https://doi.org/10.1016/j.jmmm.2008.01.004.
[26] Beltrán JI, Monty C, Balcells L, Martínez-Boubeta C. Possible d0 ferromagnetism in MgO. Solid State Commun 2009;149:1654–7. https://doi.org/10.1016/j.ssc.2009.06.044.
[27] Hassnain Jaffari G, Tahir A, Bah M, Ali A, Bhatti AS, Shah SI. Study of Surface-Active Modes and Defects in Single-Phase Li-Incorporated MgO Nanoparticles. J Phys Chem C 2015;119:28182–9. https://doi.org/10.1021/acs.jpcc.5b10131.
[28] Wang F, Pang Z, Lin L, Fang S, Dai Y, Han S. Magnetism in undoped MgO studied by density functional theory. Phys Rev B - Condens Matter Mater Phys 2009;80:1–7. https://doi.org/10.1103/PhysRevB.80.144424.
[29] Martínez-Boubeta C, Beltrán JI, Balcells L, Konstantinović Z, Valencia S, Schmitz D, et al. Ferromagnetism in transparent thin films of MgO. Phys Rev B - Condens Matter Mater Phys 2010;82:1–7. https://doi.org/10.1103/PhysRevB.82.024405.
[30] Hanish HH, Edrees SJ, Shukur MM. The effect of transition metals incorporation on the structural and magnetic properties of magnesium oxide nanoparticles. Int J Eng Trans A Basics 2020;33:647–56. https://doi.org/10.5829/IJE.2020.33.04A.16.

[31] Dasari MP, Godavarti U, Mote V. Structural, morphological, magnetic and electrical properties of Ni doped ZnO nanoparticles synthesized by co-precipitation method. Process Appl Ceram 2018;12:100–10. https://doi.org/10.2298/pac1802100d.
[32] Beltrán JI, Muñoz MC, Hafner J. Structural, electronic and magnetic properties of the surfaces of tetragonal and cubic HfO2. New J Phys 2008;10. https://doi.org/10.1088/1367-2630/10/6/063031.
[33] Gallego S, Beltrán JI, Cerdá J, Muñoz MC. Magnetism and half-metallicity at the O surfaces of ceramic oxides. J Phys Condens Matter 2005;17. https://doi.org/10.1088/0953-8984/17/43/L04.
[34] Nassar MY, Mohamed TY, Ahmed IS, Samir I. MgO nanostructure via a sol-gel combustion synthesis method using different fuels: An efficient nano-adsorbent for the removal of some anionic textile dyes. J Mol Liq 2017;225:730–40. https://doi.org/10.1016/j.molliq.2016.10.135.
[35] Jeevanandam P, Klabunde KJ. A study on adsorption of surfactant molecules on magnesium oxide nanocrystals prepared by an aerogel route. Langmuir 2002;18:5309–13. https://doi.org/10.1021/la0200921.
[36] Li WC, Lu AH, Weidenthaler C, Schüth F. Hard-templating pathway to create mesoporous magnesium oxide. Chem Mater 2004;16:5676–81. https://doi.org/10.1021/cm048759n.
[37] Type D. Nucleophilic Chemistry of the Synthesized Magnesium Oxide (Magnesia) Nanoparticles via Microwave @ sol-gel Process for Removal of Sulfurous Pollutant 2020:8–10.
[38] Zaidi B, Belghit S, Ullah MS, Hadjoudja B, Guerraoui A, Gagui S, et al. Investigation of MgO powders synthesized by liquid-phase method. Metallofiz i Noveishie Tekhnologii 2019;41:1121–6. https://doi.org/10.15407/mfint.41.08.1121.
[39] Ganapathi Rao K, Ashok C, Venkateswara Rao K, Shilpa Chakra C. Structural properties of MgO Nanoparticles: Synthesized by Co-Precipitation Technique. Int J Sci Res 2013:43–6.
[40] Mohammad Shafiee MR, Kargar M, Ghashang M. Characterization and low-cost, green synthesis of Zn2+ doped MgO nanoparticles. Green Process Synth 2018;7:248–54. https://doi.org/10.1515/gps-2016-0219.
[41] Ghorbani S, Razavi RS, Loghman-Estarki MR, Alhaji A. Development of MgO–Y2O3 Composite Nanopowder by Pechini Sol–Gel Method: Effect of Synthesis Parameters on Morphology, Particle Size, and Phase Distribution. J Clust Sci 2017;28:1523–39. https://doi.org/10.1007/s10876-017-1162-8.
[42] Tai CY, Tai C Te, Chang MH, Liu HS. Synthesis of magnesium hydroxide and oxide nanoparticles using a spinning disk reactor. Ind Eng Chem Res 2007;46:5536–41. https://doi.org/10.1021/ie060869b.
[43] Pechini MP. (Enno&P and Alway 1967.
[44] Zalapa-Garibay MA, Arizmendi-Moraquecho A, Reyes-López SY. Low temperature synthesis of alpha alumina platelets and acicular mullite in MgO-Al 2 O 3 -SiO 2 system. J Ceram Sci Technol 2019;10:9–18. https://doi.org/10.4416/JCST2018-00043.
[45] Suresh P, Babu PD, Srinath S. Effect of Ho substitution on structure and magnetic properties of BiFeO3. J Appl Phys 2014;115:2012–5. https://doi.org/10.1063/1.4863944.
[46] Leszczyński M, Litwin-Staszewska E, Suski T, Bąk-Misiuk J, Domagała J. Lattice Constant of Doped Semiconductor. Acta Phys Pol A 1995;88:837–40. https://doi.org/10.12693/aphyspola.88.837.
[47] Obeid MM, Edrees SJ, Shukur MM. Synthesis and characterization of pure and cobalt doped magnesium oxide nanoparticles: Insight from experimental and theoretical investigation. Superlattices Microstruct 2018;122:124–39. https://doi.org/10.1016/j.spmi.2018.08.015.
[48] Dussardier B, Blanc W, Mauroy V, Ude M, Trzesien S, Mady F, et al. In-Situ Grown Erbium-Doped Dielectric Nanoparticles in Silica-Based Transparent Optical Fibers. Arxiv Prepr ArXiv11012814 2011;79:2–5.
[49] Rajesh Kumar B, Hymavathi B. X-ray peak profile analysis of solid-state sintered alumina doped zinc oxide ceramics by Williamson–Hall and size-strain plot methods. J Asian Ceram Soc 2017;5:94–103. https://doi.org/10.1016/j.jascer.2017.02.001.
[50] Zhang L, Gonçalves AAS, Jaroniec M. Identification of preferentially exposed crystal facets by X-ray diffraction. RSC Adv 2020;10:5585–9. https://doi.org/10.1039/d0ra00769b.
[51] Ansari A, Ali A, Asif M, Shamsuzzaman. Microwave-assisted MgO NP catalyzed one-pot multicomponent synthesis of polysubstituted steroidal pyridines. New J Chem 2018;42:184–97. https://doi.org/10.1039/c7nj03742b.

[52] Das A, Mandal AC, Roy S, Nambissan PMG. Internal defect structure of calcium doped magnesium oxide nanoparticles studied by positron annihilation spectroscopy. AIP Adv 2018;8. https://doi.org/10.1063/1.5001105.
[53] Ke LEI, Yuan Y, Zhao HUA. Influence of Rare-Earth Doping on the Electrical. Ceramics,Silikáty 2013;57:53–7.
[54] Theophanides T. Introduction to Infrared Spectroscopy. Infrared Spectrosc - Mater Sci Eng Technol 2012. https://doi.org/10.5772/49106.
[55] Elawam S, Morsi W, Abou-Shady H, Guirguis O. Characterizations of Beta-lead Oxide “Massicot” Nano-particles. Br J Appl Sci Technol 2016;17:1–10. https://doi.org/10.9734/bjast/2016/28143.
[56] Scimeca M, Bischetti S, Lamsira HK, Bonfiglio R, Bonanno E. Energy dispersive X-ray (EDX) microanalysis: A powerful tool in biomedical research and diagnosis. Eur J Histochem 2018;62:89–99. https://doi.org/10.4081/ejh.2018.2841.
[57] Li M, Zhou S, Xu M. Graphene oxide supported magnesium oxide as an efficient cathode catalyst for power generation and wastewater treatment in single chamber microbial fuel cells. Chem Eng J 2017;328:106–16. https://doi.org/10.1016/j.cej.2017.07.031.
[58] Phokha S, Klinkaewnarong J, Hunpratub S, Boonserm K, Swatsitang E, Maensiri S. Ferromagnetism in Fe-doped MgO nanoparticles. J Mater Sci Mater Electron 2016;27:33–9. https://doi.org/10.1007/s10854-015-3713-9.
[59] Sundaresan A, Bhargavi R, Rangarajan N, Siddesh U, Rao CNR. Ferromagnetism as a universal feature of nanoparticles of the otherwise nonmagnetic oxides. Phys Rev B - Condens Matter Mater Phys 2006;74. https://doi.org/10.1103/PhysRevB.74.161306.
[60] Morozov IG, Sathasivam S, Belousova O V., Parkin IP, Kuznetcov M V. Effect of synthesis conditions on room-temperature ferromagnetic properties of Mg-O nanoparticles. J Alloys Compd 2018;765:343–54. https://doi.org/10.1016/j.jallcom.2018.06.211.
[61] Ferrari AM, Pacchioni G. Electronic structure of F and V centers on the MgO surface. J Phys Chem 1995;99:17010–8. https://doi.org/10.1021/j100046a029.
[62] Elfimov IS, Yunoki S, Sawatzky GA. Possible Path to a New Class of Ferromagnetic and Half-Metallic Ferromagnetic Materials. Phys Rev Lett 2002;89:1–4. https://doi.org/10.1103/PhysRevLett.89.216403.
[63] Kumar S, Kim YJ, Koo BH, Lee CG. Structural and magnetic properties of Ni doped CeO 2 nanoparticles. J Nanosci Nanotechnol 2010;10:7204–7. https://doi.org/10.1166/jnn.2010.2751.
[64] Brito PCA, Santos DAA, Duque JGS, Macêdo MA. Structural and magnetic study of Fe-doped CeO2. Phys B Condens Matter 2010;405:1821–5. https://doi.org/10.1016/j.physb.2010.01.054.
[65] Gupta A, Zhang R, Kumar P, Kumar V, Kumar A. Nano - Structured Dilute Magnetic Semiconductors for Efficient Spintronics at Room Temperature. Magnetochemistry 2020; 6:15. https://doi.org/10.3390/magnetochemistry6010015.